Journal of the Korean Astronomical Society
52: 83∼88, 2019 June
https://doi.org/10.5303/JKAS.2019.52.3.83
pISSN: 1225-4614 · eISSN: 2288-890X
http://jkas.kas.org

Chemical Diagnostics of the Massive Star Cluster−Forming Cloud G33.92+0.11. III. ^{13}CN and DCN

Young Chol Minh[1] and Hauyu Baobab Liu[2]

[1]Korea Astronomy and Space Science Institute, 776 Daedeok-daero, Yuseong, Daejeon 34055, Korea; minh@kasi.re.kr
[2]Academia Sinica Institute of Astronomy and Astrophysics, P.O. Box 23-141, Taipei 10617, Taiwan; hyliu@asiaa.sinica.edu.tw

Received March 5, 2019; accepted May 24, 2019

Abstract: Using ALMA observations of the ^{13}CN and DCN lines in the massive star-forming region G33.92+0.11A, we investigate the CN/HCN abundance ratio, which serves as a tracer of photodissociation chemistry, over the whole observed region. Even considering the uncertainties in calculating the abundance ratio, we find high ratios ($\gg$1) in large parts of the source, especially in the outer regions of star-forming clumps A1, A2, and A5. Regions with high CN/HCN ratios coincide with the inflows of accreted gas suggested by Liu et al. (2015). We conclude that we found strong evidence for interaction between the dense gas clumps and the accreted ambient gas which may have sequentially triggered the star formation in these clumps.

Key words: ISM: molecules — radio lines: ISM — stars: formation

1. Introduction

High-mass star formation is one of the key factors that govern the overall evolution of galaxies. Their early-phase evolutionary processes, however, are not well constrained because of the complex phenomena associated with energetic young stars forming in groups/clusters which evolve rapidly (e.g., Zinnecker & Yorke 2007; Reipurth & Yan 2008). Therefore, these massive star-forming clouds are often observed to consist of complicated sub-regions with a large variety of physical and chemical conditions. Chemical diagnostics is a powerful tool for investigating the nature of the source deeply embedded within a very dense molecular cloud (e.g., for G33.92+0.11, Liu et al. 2012, 2015, 2019; Minh et al. 2016, 2018). In this paper, we investigate the CN/HCN abundance ratio estimated from observations of the ^{13}CN and DCN lines in the massive star-forming region G33.92+0.11, to probe the photodissociation region (PDR) associated with star formation. We expect that this ratio will provide information important for understanding the cloud kinematics and the early stage of star formation.

HCN is commonly used as a tracer of dense molecular gas (with densities $n_{\rm H_2} \gtrsim 10^4$ cm^{-3}). CN is another tracer of dense gas with a lower (by a factor of five) critical density than HCN (e.g., Pérez-Beaupuits et al. 2007). Both species are known to be abundant in photodissociation regions (PDRs). A CN/HCN abundance ratio $\geq$ 1 has been suggested to be characteristic for PDRs because CN is chemically linked to HCN and can be formed by the direct photodissociation of HCN (e.g., Lafont et al. 1982; Huggins et al. 1984; Thi et al. 2004; Fuente et al. 2005). Chemical models of PDRs predict that the CN/HCN abundance ratio can be enhanced by several orders of magnitude near the ionization front (Sternberg & Dalgarno 1995; Jansen et al. 1995). The abundance ratio has been found to be enhanced substantially (up to a few) towards various sources influenced by photochemistry or shocks, as opposed to quiet regions having ratios in the range $\sim 0.01 - 0.1$ (e.g., Fuente et al. 1993, 1996, 2005; van Zadelhoff et al. 2001; Thi et al. 2004; Jørgensen et al. 2004; Öberg et al. 2010; Minh et al. 2014).

We investigate the CN/HCN abundance ratio in the massive star-forming cloud G33.92+0.11 which is located at a distance of ∼7.1 kpc (Fish et al. 2003) and viewed nearly face-on (Liu et al. 2012). The central parsec of the cloud (a region referred to as G33.92+0.11A) hosts several dense clumps, identified by their dust continuum emission at 1.3 mm (Liu et al. 2015) and associated with active star formation. These clumps consist of sub-pc-scale features with chemical properties very different from each other (Minh et al. 2016, 2018). The chemical complexity found in this region is thought to largely arise from different physical and chemical evolutionary time scales associated with massive star formation. In addition, ambient gas is still being accreted into the cloud; accordingly, the observed chemical complexity may reflect the different chemistry of ambient clouds. Gas inflows are observed as filamentary and/or arm-like features connected to the dense cores of gas clumps (Liu et al. 2015). We suspect that the accreted gas plays an important role in the very early phase of star formation.

So far, the gas inflows have not received much attention mainly because of their low densities and larger spatial extensions compared to the active dense star-forming cores. In addition, the face-on projection of the cloud makes it difficult to study the dynamics of the accretion flow. In this paper, we therefore investi-

Corresponding author: Y. C. Minh

gate signatures of interacting gas using the CN/HCN abundance ratio toward the extended features associated with star-forming cores. In Section 2, we summarize the ALMA data used for deriving this ratio and observed transitions of DCN and ^{13}CN. Section 3 includes subsections on the observed emission distributions (Section 3.1) and abundance derivations, conversion to CN and HCN abundance from the observed values (Section 3.2), and the CN/HCN abundance ratios (Section 3.3). The summary is given in Section 4.

2. DATA

We used the ALMA data (ADS/JAO.ALMA#2012.1.00387.S) taken with the 12 m array on 2014 May 4 for the DCN $3-2$ (ν=217.23863 GHz) and ^{13}CN $N=2-1$ (ν=217.46715 GHz) transitions observed toward G33.92+0.11. The same data set has been used previously by Liu et al. (2015); Minh et al. (2016, 2018). The pointing and phase referencing center was $(\alpha, \delta)_{\rm J2000}$ = ($18^{\rm h}52^{\rm m}50\overset{\rm s}{.}272$, $00^\circ55'29\overset{''}{.}604$). The frequency settings took into account a velocity of the local standard of rest of $v_{\rm lsr}$ = 107.6 km s^{-1}. Four spectral windows, two of width 234.4 MHz and two of width 1875.0 MHz, were used with channel spacings of 61 kHz and 488 kHz, respectively. The resulting angular resolution (θ) was about 0.65″ (the uv sampling range was $13-430$ kλ). The system temperatures were in range $60-150$ K and the spectral flux uncertainties of the observed lines were about $20-50$ mK (1σ). Unlike the molecular line data, the dust continuum image was taken by the ALMA 12 m + ACA array ($\theta \approx 0.67'' \times 0.47''$) and included into our analysis after subtracting the estimated contribution by free-free emission. Further observational details can be found in Liu et al. (2015).

The ^{13}CN $N=2-1$ transition splits into hyperfine transition levels, and we used the hyperfine components at 217.46715 GHz ($F_2' \rightarrow F_2 = 3 \rightarrow 2$, $F' \rightarrow F = 3 \rightarrow 2$ and $F_2' \rightarrow F_2 = 3 \rightarrow 2$, $F' \rightarrow F = 4 \rightarrow 3$) and at 217.469156 GHz ($F_2' \rightarrow F_2 = 3 \rightarrow 2$, $F' \rightarrow F = 2 \rightarrow 1$). The 217.46715 GHz and 217.469156 GHz components are responsible for 27.7% and 6.0% of the total $N = 2-1$ emission, respectively (Flower & Hily-Blant 2015), separated by $\Delta v = -2.76$ km s^{-1}.

3. RESULTS AND DISCUSSION

3.1. Spatial Distribution of Emission

G33.92+0.11A consists of several dense clumps containing massive star-forming cores. Figure 1 shows the dust emission distribution in the G33.92+0.11A region, which roughly traces the total gas density of the region weighted by the dust temperature. The physical conditions of these cores have been studied in detail by Liu et al. (2015, 2019). The most prominent gas clumps are associated with the dust emission peaks A1, A2, and A5 where massive stars are forming (e.g., Liu et al. 2012, 2015; Minh et al. 2016). The A1 clump is associated with an ultra-compact (UC) HII region originating from the massive star cluster formed which was part of the first generation of stars formed in the cloud. The most recent star formation is observed to occur in the A5 clump, as indicated by the existence of multiple SiO outflows and hot cores (Minh et al. 2016).

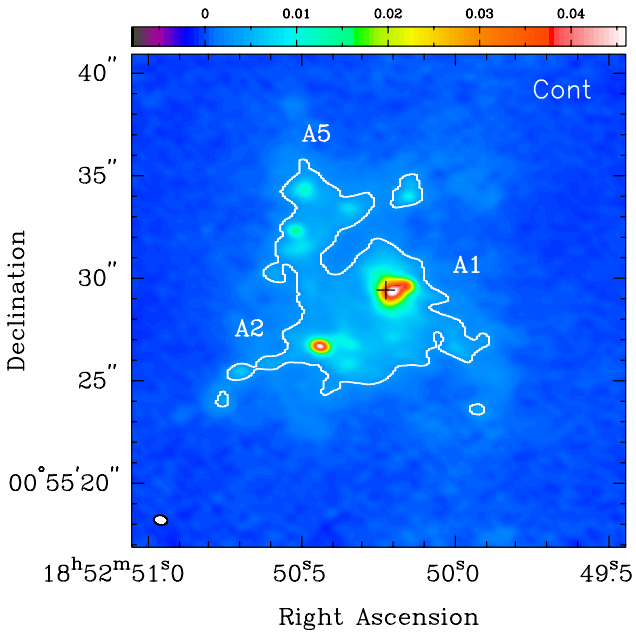

Figure 1. Continuum map at 1.3mm (after subtracting a free-free emission model, Liu et al. 2015). The intensity scale at the top is in units of Jy beam^{-1}. The white contour line marks a continuum emission strength of 3 mJy beam^{-1}. A1, A2, and A5 indicate the clumps containing the dust emission peaks number 1, 2, and 5 of G33.92+0.11A, respectively (Liu et al. 2012). The black cross denotes the position of the UC HII region.

Figures 2 and 3 show the spatial distributions of the DCN $3-2$ and ^{13}CN $N=2-1$ emission, respectively, smoothed to a resolution of about 1″ resolution, i.e. roughly the half-power size of the identified sub-cores (Minh et al. 2018). We included a sample spectrum in each figure taken toward the peak emission position, taken at the same spatial resolution of 1″. The line parameters are listed in Table 1.

The DCN emission in Figure 2 shows a good correlation with the dust emission in Figure 1 as previously noted by Liu et al. (2015). DCN is deuterated hydrogen cyanide (HCN) which is thought to control the nitrogen chemistry in the gas phase, its deuterium fractionation is known to proceed efficiently in dense gas (e.g., Rodgers & Charnley 2001; Gerlich et al. 2002). As discussed by Minh et al. (2018), DCN can form efficiently not only in cold gas through typical gas phase deuteration reactions initiated by H_2D^+, but also in the warm dense core either by evaporation of the depleted DCN from ice grain mantles or by lukewarm gas phase deuterium fractionation of HCN associated with CH_2D^+. This seems to explain why DCN is observed allover massive star-forming regions with relatively constant abundances over the observed regions (a few $\times 10^{-10} - 10^{-11}$, e.g., Roberts et al. 2002; Parise et al. 2009; Ginard et al. 2012; Ren et al. 2012).

However, the ^{13}CN emission in Figure 3 shows a

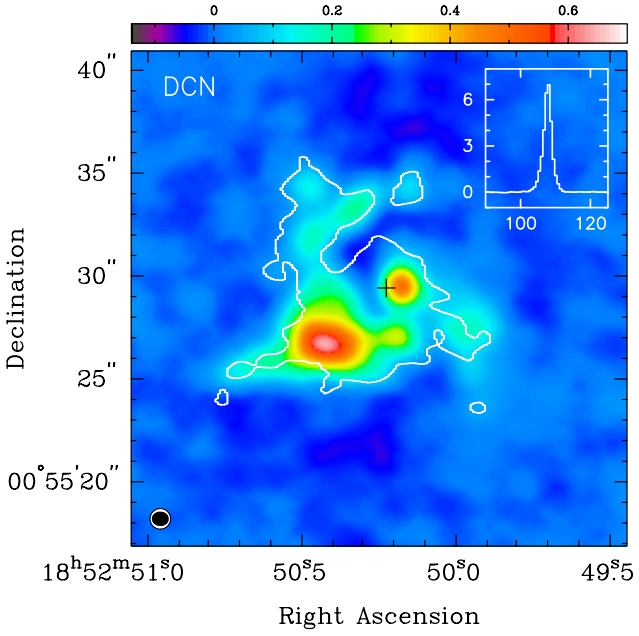

Figure 2. Map of the integrated intensity of DCN $3-2$. The intensity scale (in units of Jy beam^{-1} km s^{-1}) is shown at the top. The white contour outlines the continuum emission shown in Figure 1. The black cross marks the position of the UC HII region. A sample spectrum taken at the position of the emission peak $(\alpha,\ \delta)_{\rm J2000} = (18^{\rm h}52^{\rm m}50\overset{\rm s}{.}42,\ 00^\circ55'26\overset{''}{.}66)$ is shown in the inset in the top-right corner. Its abscissa shows $v_{\rm lsr}$ (in km s^{-1}) and its ordinate shows the flux density (in K).

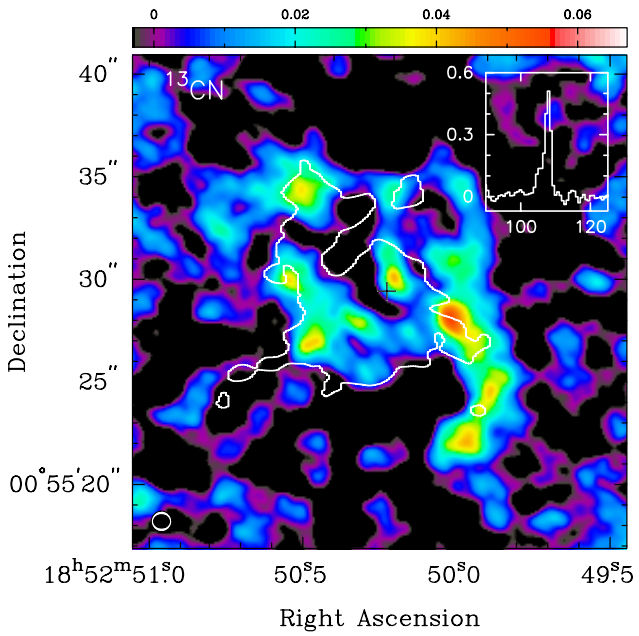

Figure 3. Same as Figure 2 but for ^{13}CN $N = 2-1$. The emission peak is located at $(\alpha,\ \delta)_{\rm J2000} = (18^{\rm h}52^{\rm m}50\overset{\rm s}{.}02,\ 00^\circ55'28\overset{''}{.}12)$.

distribution very different from that of the DCN emission and also from those of other molecules such as, for example, CS, SiO, CH_3OH, etc., reported previously (e.g., Liu et al. 2015; Minh et al. 2016, 2018). We think that this difference results from the PDR chemistry of CN, which is largely different from the chemistry related to other species including HCN. As the abundance ratio of CN and HCN is thought to be a good tracer of PDRs, we expect that this ratio will provide an interesting information for the cloud kinematics associated with the activities of massive star formation.

3.2. Abundances

We first calculated the DCN and ^{13}CN abundances from the data assuming optically thin emission and local thermodynamic equilibrium (LTE). These values were converted to HCN and CN abundances by applying the estimated D/H and ^{12}C/^{13}C abundance ratio, respectively. For the derivation of the DCN and ^{13}CN abundances we used the relation

$$N_{\rm column} = (2\pi\nu^2 k/hc^3 f_u A) \int T_R^* d\nu \qquad (1)$$

(cf. Irvine et al. 1987), where ν is the line frequency, k is the Boltzmann constant, $\int T_R^*\, d\nu$ is the integrated brightness temperature of the line, h is the Planck constant, c is the speed of light, f_u is the fractional population of the upper level of the line, and A is the Einstein coefficient of the line. For calculationg the fractional population f_u, we used rotational temperatures in the range $T_{\rm rot} = 20...50$ K, estimated from our previous works (Liu et al. 2012, 2019; Minh et al. 2016). The total uncertainties resulted from the $T_{\rm rot}$ range and the observed spectral root-mean-squared errors (3σ) were added in quadrature and listed in the last column of Table 1 as percentage of the total column density.

For the derivation of the CN/HCN abundance ratio, we converted the observed abundances of ^{13}CN and DCN to those of CN and HCN by applying the expected isotope ratio of ^{12}C/^{13}C and D/H to the observed results, respectively. The cosmic value of the ^{12}C/^{13}C abundance ratio is 89, but the molecular abundance ratios between the species containing ^{12}C and ^{13}C have been found to be in the range $10-80$ depending on the source (e.g., Wilson & Rood 1994; Bakker & Lambert 1998; Roueff et al. 2015; Ritchey et al. 2018). We applied a ^{12}CN/^{13}CN abundance ratio of 40 to derive the CN abundance from the ^{13}CN results. In addition to the $20-30\%$ uncertainty of the ^{13}CN abundance listed in Table 1, we expect that the isotope conversion will provide an additional uncertainty of a few tens % of the ^{12}CN abundance. This estimate applies similarly to the final HCN abundance discussed below. Therefore, the final abundance ratio of CN/HCN will be uncertain by a factor of a few. For this reason, instead of discussing the accurate value of this ratio, we focus on the relative abundance ratio distribution over the whole observed region to distinguish the properties associated with massive star formation.

For estimating the HCN abundance, we applied the expected DCN/HCN abundance ratio to the DCN abundance. The cosmic D/H abundance ratio is about 10^{-5}

Table 1
Line parameters for the spectra in Figures 2 and 3 and abundances

Molecule	$v_{\rm lsr}^{\rm a}$ (km s^{-1})	$T_{peak}^{\rm a}$ (K)	Δv (HPW)$^{\rm a}$ (km s^{-1})	$\int T\,dv$ (K km s^{-1})	rms (1σ) (mK)	$N_{\rm column}^{\rm d}$ (cm^{-2})
DCN	107.7	6.7	2.8	21.9	34	2.4×10^{13} ±15%
^{13}CN	107.9$^{\rm b}$/105.6$^{\rm c}$	0.50$^{\rm b}$/0.13$^{\rm c}$	1.7$^{\rm b}$/2.6$^{\rm c}$	1.5	29	4.6×10^{13} ±27%

[a]From fitting Gaussian profiles.
[b]For the hyperfine components $F_2' \rightarrow F_2 = 3 \rightarrow 2$, $F' \rightarrow F = 3 \rightarrow 2$ & $F_2' \rightarrow F_2 = 3 \rightarrow 2$, $F' \rightarrow F = 4 \rightarrow 3$ at 217.46715 GHz.
[c]For the hyperfine components $F_2' \rightarrow F_2 = 3 \rightarrow 2$, $F' \rightarrow F = 2 \rightarrow 1$ at 217.469156 GHz. The $v_{\rm lsr}$ value is calculated with respect to the rest frequency of the strongest component which is 217.46715 GHz.
[d]Column density uncertainties are given in percentages, using the rotational temperature range $20 - 50$ K and the spectral rms value (3σ) which were added in quadrature.

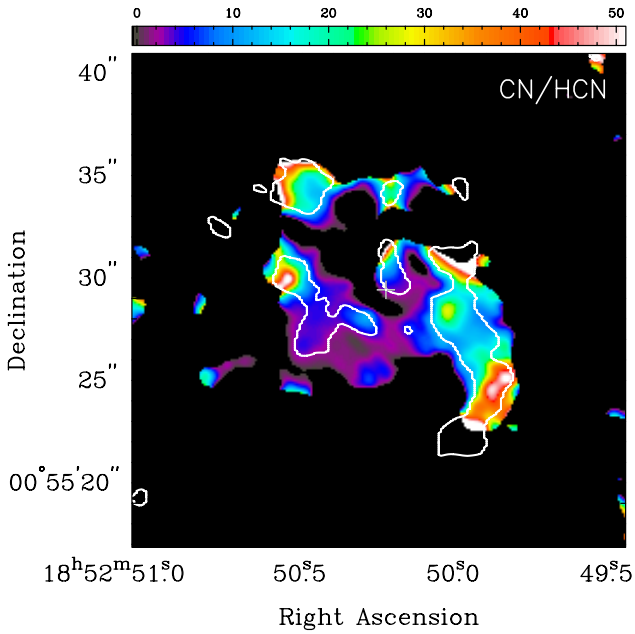

Figure 4. Column density ratio of CN/HCN derived from ^{13}CN and DCN intensities. The color bar at the top shows the range of abundance ratios. The white cross marks the position of the UC HII region. The white contour is the 0.02 Jy beam^{-1} km s^{-1} strength of the CN $N = 2$ line emission in Figure 3.

but efficient deuterium fractionation occurs in dense molecular clouds (e.g., Linsky et al. 1993; Oliveira et al. 2003). Especially, HCN shows a high degree of deuterium fractionation in warm gas, as described in the introduction (and the references in Minh et al. 2018). The DCN/HCN abundance ratio has been found to be in the range $0.02 - 0.1$ from observations towards various different sources and also from chemical modelling (e.g., Roberts et al. 2002; Öberg et al. 2010; Gerner et al. 2015). We used a DCN/HCN abundance ratio of 0.05 to derive the HCN abundance from that of DCN. Although most of the uncertainties of the ^{13}CN and DCN data will cancel out when deriving the abundance ratios since the lines were taken simultaneously and have similar frequencies, we expect that the resulting abundance ratios will still have large uncertainties up to a factor of a few, as mentioned above.

3.3. The CN/HCN Abundance Ratio

Even though large uncertainties in the final CN/HCN abundance ratio are likely to persist, it is apparent that the ratio is $\gg$1 over a significant part of the source, as shown in Figure 4. The ratio was calculated only for map pixels which have both a positive CN flux and a DCN intensity $\geq$20 mJy beam^{-1} km s^{-1}. Considering the uncertainties, the values < 10 near the dense star-forming cores are up for debate. However, for the regions with ratios $\geq$10 we can say for sure that their CN/HCN ratios are enhanced compared to quiet regions. The regions with high ratios are located outside of dense clumps and coincide with the postulated accretion flow filaments.

As summarized in Section 1 for the CN/HCN ratio, the major formation routes of CN are thought to be either photodissociation of HCN or photochemistry involving atomic C and N. However, G33.92+0.11A is the central part of a larger molecular cloud and is unlikely to be affected by photons from the interstellar radiation field. The newly formed stars are also embedded deeply in the dense cores. Therefore, along with the morphology of the region having a high CN/HCN ratio (Figure 4), we expect that strong shocks caused by the interaction of accreted gas and the existing clumps generate the photons and physical conditions necessary for the enhancement of the CN/HCN ratio, although the shocks or phases of elevated temperatures or densities only last for a short time – with the relaxation time scale being of the order of hundred years. This argument can also be applied to the high value of the abundance ratio in the outer region of a protoplanetary disk (e.g., Thi et al. 2004).

The most prominent feature in our map is an arc-like gas filament pointing south from the clump A1. This filament is likely to be gas accreted toward A1 from the ambient medium (Liu et al. 2015). Since the total column density of this filamentary feature is low compared to other dense regions, as estimated from the dust emission (Figure 1), we suppose that the enhanced CN abundance and also the CN/HCN ratio along this component result from shocks formed in the accretion process which may have triggered the first star formation in the A1 clump.

This first star formation has formed the UC HII region marked by a cross in our figures. PDRs may have

been formed by the young stellar objects associated with the UC HII region. The CN/HCN ratio is, however, found to be low near this region. Since this UC HII region is embedded in the dense gas cloud, we expect that there may exist a shallow PDR of which the total CN column density may not be large enough compared to the DCN abundance in the line of sights. The DCN abundance could have been enhanced in warm dense gas compared to the ambient region (Minh et al. 2018). On the other hand, CN appears to be more abundant in relatively extended and less dense gas as seen in Figure 3.

We also found a high abundance ratio in the northern part of the A2 clump. The region showing a high ratio is located outside of the dense core where star formation is taking place (Minh et al. 2016). We expect that the accreted gas is falling toward A2, as suggested by Liu et al. (2015), and is interacting with A2. The large abundance ratio compared to the A5 clump, especially in the northern part of this clump, is thought to result mainly from the interaction between the accreted gas and the star-forming core where star formation is taking place, as indicated by strong multiple SiO outflows and the existence of hot cores (Minh et al. 2016). It is also possible that the star formation in A5 is triggered by recent accretion of gas from the northern direction (Liu et al. 2015; Minh et al. 2016).

The regions with high abundance ratios coincide with the flows of accreted gas described by Liu et al. (2015, Figure 15). Because of the almost face-on orientation of the source, there is no clear evidence for accreted gas which would be extended and less dense than the star-forming cores. Given the difficulties of tracing cloud-cloud interactions or the triggering processes of star formation, we consider the CN/HCN ratio a good tracer of the environment of PDRs. Information on interactions between dense cores and ambient gas can be important to understand the early phase of cloud formation and the sequential formation of massive stars in the associated dense gas clumps.

4. Summary

Using ^{13}CN and DCN ALMA line maps, we investigated the CN/HCN abundance ratio, which serves as a tracer of photodissociation chemistry, in G33.92+0.11A. Despite large uncertainties, large ratios (>10), which clearly suggest enhanced CN/HCN ratios relative to the quiet dense gas, have been found in the outer regions of the star-forming clumps A1, A2, and A5. These regions coincide with the expected flows of accreted gas toward the dense clumps (Liu et al. 2015) and PDRs may have formed during the accretion process. This is evidence for accreted gas–cloud interactions which may also have triggered the star formation in the gas clumps.

Acknowledgments

ALMA is a partnership of ESO (representing its member states), NSF (USA) and NINS (Japan), together with NRC (Canada), MOST and ASIAA (Taiwan), and KASI (Republic of Korea), in cooperation with the Republic of Chile. The Joint ALMA Observatory is operated by ESO, AUI/NRAO and NAOJ.

References

Bakker, E. J. & Lambert, D. L. 1998, The Circumstellar Shell of the Post-Asymptotic Giant Branch Star HD 56126: The ^{12}CN/^{13}CN Isotope Ratio and Fractionation, ApJ, 508, 387

Fish, V. L., Reid, M. J., Wilner, D. J., & Churchwell, E. 2003, HI Absorption toward UC HII Regions: Distances and Galactic Structure, ApJ, 587, 701

Flower, D. R. & Hily-Blant, P. 2015, Hyperfine Transitions of ^{13}CN from Pre-protostellar Sources, MNRAS, 452, 19

Fuente, A., Martín-Pintado, J., Cernicharo, J., & Bachiller, R. 1993, A Chemical Study of the Photodissociation Region NGC 7023, A&A, 276, 473

Fuente, A., Rodríguez-Franco, A., & Martín-Pintado, J. 1996, Chemistry in the High Density Molecular Interface Surrounding the Orion Nebula, A&A, 312, 599

Fuente, A., Garsía-Burillo, S., Gerin, M., et al. 2005, Photon-Dominated Chemistry in the Nucleus of M82: Widespread HOC^+ Emission in the Inner 650 Parsec Disk, ApJ, 619, L155

Gerlich, D., Herbst, E., & Roueff, E. 2002, H_3^++HD→ H_2D^++H_2: Low-temperature Laboratory Measurements and Interstellar Implications, Planet. Space Sci., 50, 1275

Gerner, T., Shirley, Y. L., Beuther, H., et al. 2015, Chemical Evolution in the Early Phases of Massive Star Formation II. Deuteration, A&A, 579, A80

Ginard, D., González-García, M., Fuente, A., et al. 2012, Spectral Line Survey of the Ultracompact H II Region Monoceros R2, A&A, 543, A27

Huggins, P. J., Glassgold, A. E., & Morris, M. 1984, CN and C_2H in IRC +10216, ApJ, 279, 284

Irvine, W. M., Goldsmith, P. F., & Hjalmarson, Å. 1987, Chemical Abundances in Molecular Clouds, in Interstellar Processes, ed. Hollenbach, D. J. & Thronson Jr., H. A. , Astrophys. Space Sci. Libr., 134, 561

Jansen, D. J., van Dishoeck, E. F., Black, J. H., et al. 1995, Physical and Chemical Structure of the IC 63 Nebula II. Chemical Models, A&A, 302, 223

Jørgensen, J. K., Schöier, & van Dishoeck, E. F. 2004, Imaging Chemical Differentiation around the Low-Mass Protostar L483-mm, ApJ, 416, 603

Lafont, S., Lucas, R., & Omont, A. 1982, Molecular Abundances in IDC +10216, A&A, 106, 201

Linsky, J. L., Brown, A., Gayley, K., et al. 1993, Goddard High-resolution Spectrograph Observations of the Local Interstellar Medium and the Deuterium/Hydrogen Ratio along the Line of Sight toward Capella, ApJ, 402, 694

Liu, H. B., Chen, H. V., Román-Zúñiga, C. G., et al. 2019, Investigating Fragmentation of Gas Structures in OB Cluster-forming Molecular Clump G33.92+0.11 with 1000 au Resolution Observations of ALMA, ApJ, 871, 185

Liu, H. B., Galvañ-Madrid, R., Jimeńez-Serra, I., et al. 2015, ALMA Resolves the Spiraling Accretion Flow in the Luminous OB Cluster-forming Region G33.92+0.11, ApJ, 804, 37

Liu, H. B., Jiménez-Serra, I., Ho, P. T. P., et al. 2012, Fragmentation and OB Star Formation in High-Mass Molecular Hub-Filament Systems, ApJ, 756, 10

Minh, Y. C., Kim, K.-T., Yan, C.-H., et al. 2014, Properties of the Molecular Clump and the Associated UC HII Region in the Gas Shell of the Expanding H II Region Sh 2-104, JKAS, 47, 179

Minh, Y. C., Liu, H. B., & Galvań-Madrid, R. 2016, Chemical Diagnostics of the Massive Star Cluster-forming Cloud G33.92+0.11. I. ^{13}CS, CH_3OH, CH_3CN, OCS, H_2S, SO_2, and SiO, ApJ, 824, 99

Minh, Y. C., Liu, H. B., Galvań-Madrid, R., et al. 2018, Chemical Diagnostics of the Massive Star Cluster-forming Cloud G33.92+0.11. II. HDCS and DCN, ApJ, 864, 102

Öberg, K. I., Qi, C., Fogel, J. K. J., et al. 2010, The Disk Imaging Survey of Chemistry with SMA. I. Taurus Protoplanetary Disk Data, ApJ, 720, 480

Oliveira, C. M., Hébrard, G., Howk, J. C., et al. 2003, Interstellar Deuterium, Nitrogen, and Oxygen Abundances toward GD 246, WD 2331-475, HZ 21, and Lanning 23: Results from the FUSE Mission, ApJ, 587, 235

Parise, B., Leurini, S., Schilke, P., et al. 2009, Deuterium Chemistry in the Orion Bar PDR. "Warm" Chemistry Starring CH_2D^+, A&A, 508, 737

Pérez-Beaupuits, J. P., Aalto, S., & Gerebro, H., 2007, HNC, HCN and CN in Seyfert Galaxies, A&A, 476, 177

Reipurth, B. & Yan, C.-H. 2008, in ASP Conf. Ser. 402, Handbook of Star Forming Regions: Vol. I. The Northern Sky, ed. Reipurth, B. (San Francisco, CA: ASP), 869

Ren, Z., Wu, Y., Zhu, M., et al. 2012, The Molecular Emissions and the Infall Motion in the High-mass Young Stellar Object G8.68-0.37, MNRAS, 422, 1098

Ritchey, A. M., Federman, S. R., & Lambert, D. L. 2018, Interstellar CN and CH^+ in Diffuse Molecular Clouds: $^{12}C/^{13}C$ Ratios and CN Excitation, ApJ, 728, 36

Roberts, H., Fuller, G. A., Millar, T. J., et al. 2002, A Survey of [HDCO]/[H_2CO] and [DCN]/[HCN] Ratios Towards Low-mass Protostellar Cores, A&A, 381, 1026

Rodgers, S. D. & Charnley, S. B. 2001, Chemical Differentiation in Regions of Massive Star Formation, ApJ, 546, 314

Roueff, E., Loisin, J. C., & Hickson, K. M. 2015, Isotopic Fractionation of Carbon, Deuterium, and Nitrogen: A Full Chemical Study, A&A, 576, A99

Sternberg, A., & Dalgarno, A. 1995, Chemistry in Dense Photon-dominated Regions, ApJS, 99, 565

Thi, W.-F., van Zadelhoff, G.-J., & van Dishoeck, E. F. 2004, Organic Molecules in Protoplanetary Disks around T Tauri and Herbig Ae Stars, A&A, 425, 955

van Zadelhoff, G.-J., van Dishoeck, E. F., Thi, W. F., & Blake, G. A. 2001, Submillimeter Lines from Circumstellar Disks around Pre-main Sequence Stars, A&A, 377, 566

Wilson, T. L. & Rood, R. T. 1994, Abundances in the Interstellar Medium, ARAA, 32, 191

Zinnecker, H. & Yorke, H. W. 2007, Toward Understanding Massive Star Formation, ARAA, 45, 481